J Nanopart Res (2020) 22: 79
https://doi.org/10.1007/s11051-020-04790-1

RESEARCH PAPER

Impact of graphene oxide nano sheets loaded with chemotherapeutic drug on tumor cells

Lobna Assy · Ali Gemeay · Soha Gomaa · Maha A. Aldubayan · Mohamed L. Salem

Received: 10 January 2020 / Accepted: 21 February 2020 / Published online: 25 March 2020

Abstract Graphene oxide (GO) nanosheet is a drug delivery system due to its structural properties, which can be augmented in presence of folic acid (FA). This study aimed to compare the efficacy of GO as a passive (GO/DOX) and active (GO/FA/DOX) forms for delivering doxorubicin (DOX). These two forms of conjugates were characterized before and after loading of DOX to confirm the conjugation as well as their properties including size and thermal stability. Using Ehrlich ascites carcinoma (EAC) cell line, the antitumor effect was evaluated by MTT assay in vitro and cell count; tumor cell cycle and apoptosis were evaluated by flow cytometry in vivo. The results showed that the loading percentages of DOX onto GO (GO/DOX) and GO/FA/DOX were 91% and 83%, respectively. TEM, FT-IR, and TGA confirmed the nano size, physical conjugation by shifted groups, and thermal stability. In vitro, the conjugates induced similar decrease of EAC cell viability, but still lower than those of free DOX. Treatment of EAC-bearing mice with GO/DOX or GO/FA/DOX forms induced significant decreases of the total numbers of EAC cells by 79% and 97%, respectively, as compared with free DOX (97%). DOX, GO/DOX, and GO/FA/DOX induced cell cycle arrest at G0, G1, and S phase, respectively. These conjugates also induced significant apoptosis with different profiles on viable, early, and late apoptotic EAC cells. In conclusion, loading DOX on GO nanosheet activated with FA can induce antitumor effect similar to those of free DOX but with different mechanisms.

Keywords Antitumor · Cancer · Doxorubicin · Ehrlich ascites · Environmental and health effects · Folic acid · Graphene oxide · Nanosheets

This article is part of the topical collection: Nanotechnology in Arab Countries

Guest Editor: Sherif El-Eskandarany

L. Assy · S. Gomaa · M. L. Salem
Immunology and Biotechnology Unit, Department of Zoology, Faculty of Science, Tanta University, Tanta, Egypt

L. Assy (✉) · M. L. Salem
Center of Excellence in Cancer Research, Tanta University, Teaching Hospital, Tanta University, Tanta, Egypt
e-mail: lobnaismailassy@gmail.com

A. Gemeay
Department of Chemistry, Faculty of Science, Tanta University, Tanta, Egypt

M. A. Aldubayan
Pharmacology and Toxicology Department College of Pharmacy, Qassim University, Buraydah, Kingdom of Saudi Arabia

Introduction

Graphene oxide (GO), a form of graphene, belongs to carbon nanoparticles family as graphite, fullerenes, and carbon nano tubes (Geim and Novoselov 2007). GO structure consists of a single atom thick sheet of sp^2 hybridized carbon atoms arranged in a hexagonal lattice. The carbon atoms in GO are attached together via covalent bonds in the same plane, forming sheets arranged through weak Van der Waal forces (Muazim and Hussain 2017). This structure of GO provides remarkable large surface area, physical, chemical, good thermal, and

electrical conductivity properties, which make GO suitable substrate for functionalization through covalent (Khan et al. 2017) and non-covalent methods (Siriviriyanun et al. 2015) as hydrogen bonding, π- π stacking, hydrophobic and electrostatic interactions without chemical interactions which may lead to critical manipulations of the structure. GO has been used in several studies to deliver different drugs including doxorubicin (DOX). Structurally, DOX consists of a tetracyclic ring with the sugar daunosamine attached by a glycosidic linkage and is considered a wide spectrum of activity and is being used as standard chemotherapeutic agent against solid tumors (Minotti et al. 2004). DOX belongs to the class of cycle-phase nonspecific drugs which can kill tumor cells with a variety of cell cycles (Coffelt and de Visser 2015). Taken together, the structure and properties of GO and DOX, GO-based materials can enhance the potential use of GO as a drug delivery carrier especially for cancer therapeutic drugs.

The drug delivery properties of GO can be further enhanced after its conjugation with a ligand that specifically bind to its receptor on the target cells. This form of GO is considered an active form. The active forms of GO are used as a target drug delivery system through receptor-mediated endocytosis (Stella et al. 2000) with the main goal to target cancer cells through certain receptors that are rich on cancer cells but not healthy cells (Bhatia 2016). With this regard, several ligands can be used as molecular signatures on the surface of cancer cells (Kim et al. 2015), including peptides (Nasongkla et al. 2004), transferrin (Daniels et al. 2006), polysaccharides (Janes et al. 2001), monoclonal antibodies (Dinauer et al. 2005), and folic acid (FA) (Licciardi et al. 2006).

The main goal of this study was to compare the antitumor effects of GO loaded with DOX in a passive (GO/DOX) and an active (rGO/FA/DOX) forms with those of free DOX as well as to explore whether they have different or similar mechanistic effects on tumor cell apoptosis and cell cycle as described in schematic diagram (Fig. 1). Our results indicate that the passive and active forms of GO/DOX conjugates induce similar antitumor effects but with different profiles on cell cycle and apoptosis.

Materials and methods

Reagents and antibodies

Graphite power (~ 60 meshes, 98% purity) was purchased from LOBA Chemie, India and was used as received. Potassium permanganate, potassium dihydrogen phosphate, sodium hydrogen phosphate, sulfuric acid (97–99%), methanol, hydrogen peroxide (30%v/v) and dimethylsulfoxide (DMSO), phosphoric acid, and hydrochloric acid (30–34%) were obtained from SDFCL, folic acid from El-Nasr Pharma (Chem. Co, Egypt). Buffered phosphate saline (PBS), complete RPMI-1640 medium with amino acids, antibiotics, and MTT (3-(4, 5-dimethylthiazol-2-yl)-2, 5-diphenyltetrazolium bromide) were purchased from Sigma (Cairo, Egypt). Triton 100X, RNase, Propodium iodide (PI), and annexin V, used for cell cycle and apoptosis analysis, were purchased from BD biosciences (CA, USA). Ehrlich ascites carcinoma (EAC) cell line was purchased from the National Cancer Institute (Cairo, Egypt) and maintained in the ascetic form by sequential passages in female Swiss albino mice by means of biweekly intraperitoneal (i.p.) injection of 2.5×10^6 tumor cells/mouse suspended in 0.1 ml PBS.

Synthesis of GO

The Hammer's improved method is utilized for the synthesis of GO Marcano et al. (2010). Typically, 9:1 mixture of H_2SO_4/H_3PO_4 (360:40 ml) was added to 3 g of graphite powder. After a quiet stirring, 18 g $KMnO_4$ was added gradually producing a slight exothermic ~ 35–40 °C. The reaction was then warmed to 50–55 °C and stirred continuously for 24 h. After the suspension color change from black to brown, the reaction was cooled to room temperature before it was transferred onto cold water 500 ml with 5 ml of 30%v/v H_2O_2. For work-up, the mixture was then washed in sequence with 100 ml of 30% HCl, demineralized water numerous times, and the supernatant was decanted away after being checked for sulfate, phosphate, and chloride ions. The remaining solid material was dried overnight at 60 °C, obtaining ~ 5 g of GO powder.

Loading FA on GO

One milligram of FA was dissolved into 10 ml of deionized water having 4 drops of hydrazine monohydrate and simply mixed with aqueous GO solution (1 mg in 10 ml of deionized water), resulting in solution of GO/FA mixture. Chemical reduction of GO/FA mixture with 4 drops of hydrazine monohydrate was performed at 80 °C for 4, 8, or 12 h. To remove excess hydrazine and any nonconjugated FA from rGO/FA conjugate, ultracentrifugation was performed at 12000 rpm,

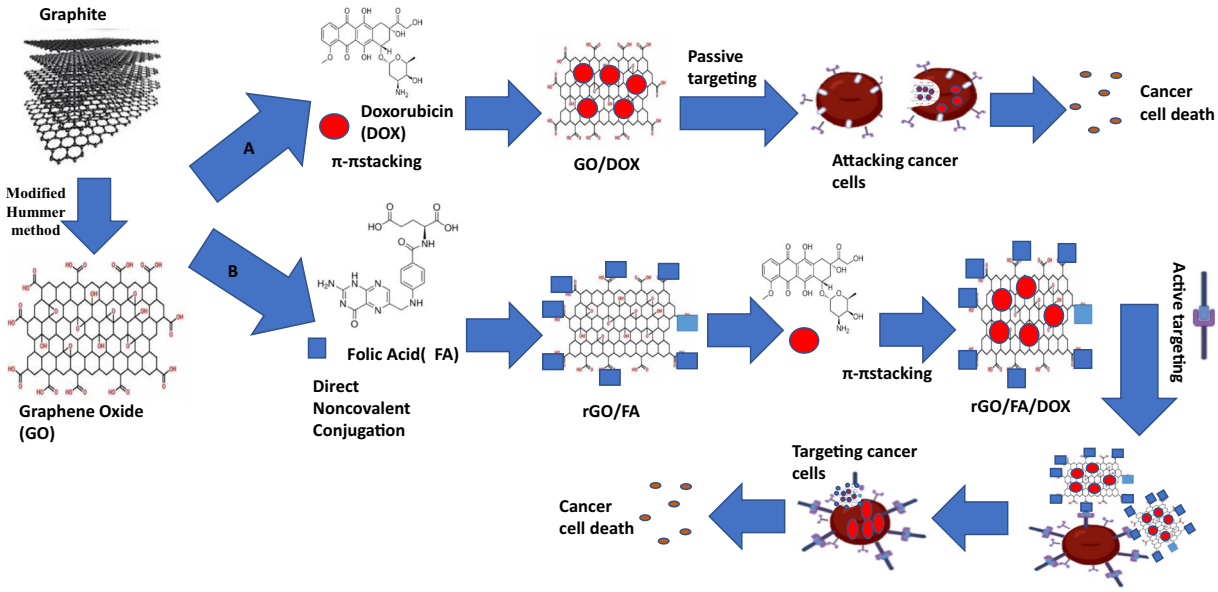

Fig. 1 Schematic diagram demonstrating the synthesis of GO/DOX (passive form; upper panel) and GO/FA/DOX (active form; lower panel)

forming precipitation of rGO/FA conjugate, which is readily dispersible again in aqueous media.

DOX loading performance of GO and rGO/FA conjugate

DOX (1 mg ml^{-1}) in H_2O was added to GO or rGO/FA (1 mg ml^{-1}) conjugate solution (0.05 mg/ml^{-1}) in phosphate buffered saline (PBS) at pH 7.4 under vigorous stirring for 12 h under dark condition. Unconjugated DOX was removed by centrifugation at 12000 rpm. The DOX concentration after centrifugation was calculated from a calibration curve which is obtained by measuring the absorbance at $\lambda_{max} = 480$ nm in UV-Vis spectrophotometer of several DOX solutions with known concentrations. Subtraction of the DOX concentration from the initial concentration of DOX added into the solution of GO or rGO/FA conjugate provides DOX loading efficiency of rGO/FA conjugate. The DOX loading percentage was measured via the absorbance at $\lambda_{max} = 490$ nm and calculated using Eq. (1):

$$\text{Loading}\% = \frac{C_0 - C_{sup}}{m_{GO}} \times 100 \quad (1)$$

where C_o represents the concentration of DOX, C_{sup}, the concentration of DOX in the supernatant after reaction, and m_{GO}, the mass of GO. The calculated dose–response curve of DOX content according to the standard curve of absorbance versus DOX concentration was plotted.

Experimental animals

Female Swiss albino mice (6-weeks old and weighed 20 ± 3 g) were obtained from Company for Biological Products and Vaccines (VACSERA), Cairo, Egypt. All mice were housed at animal unit, Zoology Department, Faculty of Science, Tanta University, Egypt upon the approval of the institutional ethical committee. All animals were housed under the same environmental conditions for 1 week before experimentation for acclimatization. Mice were housed under standard laboratory conditions (temperature 22 °C ± 2 °C; 12 h light-dark cycle) and kept in plastic cages with free access to the commercial basal food and water.

In vitro cytotoxicity of conjugates

In vitro, cytotoxicity of EAC cells was done using MTT assay. Briefly, EAC cells suspended in complete RPMI-1640 medium then, seeded in 96 well plates at a density of 1×10^4 cells per well. After 24 h, GO, GO/DOX, or rGO/FA/DOX conjugates were added to the cultured cells at the concentration of 50 μg/ml for 48 h. Then, the supernatants were removed and the 10 μl MTT was added and kept for further 4 h. After discarding the supernatant, the formazan crystals were solubilized with 200 μl DMSO for 15–

30 min. The optical density (OD) of solutions was then read at 540 nm by spectrophotometer (ELx 808 ultra-microplate reader, Bio-Tek instruments, USA). Triplicate of each sample was done and untreated cells were served as negative control. A blank was performed in parallel to monitor the influence of RPMI-1640 medium on the assays. The cell viability was calculated as follows:

$$\text{Tumor cell viability}\% = \text{OD (test)} - \text{OD (blank)} / \text{OD (control)} - \text{OD (blank)} \times 100$$

In vivo antitumor effects of conjugates

Naïve female mice were implanted with i.p. injection of 2.5×10^5 EAC cells/mouse and then divided randomly into designated groups ($n = 9$/group). One day later, EAC-bearing mice were treated with PBS, 300 μl DOX (15 mg/kg), GO/DOX, and rGO/FA/DOX. While DOX concentration in the conjugates was adjusted at 15 mg/kg (Osman et al. 2013). All mice were sacrificed on day 10 post EAC inoculations by cervical dislocation.

Measuring cell cycle of EAC cells by flow cytometry

EAC cells were harvested from EAC-bearing mice, which were treated with PBS, DOX, GO/DOX, or rGO/FA/DOX, washed twice with ice-cold PBS, and fixed with 70% ethanol at 4 °C overnight. The fixed cells were resuspended in 300–500 μl PI/triton X 100 staining solution (1000 μl of 0.1% triton + 40 μl PI + 20 μl RNAse), for 30 min at 37 °C in the dark. The cells were then centrifuged at 1000×*g* and the number of cells at the different phases of the cell cycle was analyzed using flow cytometry (BD FACSCanto II flow cytometry (BD Biosciences, USA) and the data were analyzed using the BD FACS Diva software).

Measuring apoptosis of EAC cells by flow cytometry

EAC cells were collected from EAC-bearing mice that were previously treated with PBS, DOX, GO/DOX, or rGO/FA/DOX. EAC cells were washed twice with ice-cold PBS, the cell density was calculated, and the cells were resuspended in 1X annexin-binding buffer to obtain a final density of 1×10^6 cells/ml. One hundred microliter of the cell suspension was placed into 1.5-ml eppendorf tubes and 5-μL annexin V-fluorescein isothiocyanate (FITC), and 1 μL PI (100 μg/ml) working solution was added. Stained EAC cells were then incubated at room temperature for 15 min followed by addition of 400 μL of 1X annexin-binding buffer with gentle mixing then the samples kept on ice. The cells were then analyzed by flow cytometry.

Statistical analysis

The data were presented as mean ± standard error of the mean. Statistical comparisons among prospective groups were analyzed using the one-way analysis of variance (ANOVA) as part of the SPSS software package (v.16.0 for Windows, 2007; SPSS, Inc., Chicago, IL). Statistical significance was determined by a post hoc test followed by Dunnett's multiple comparison tests to compare treatment means with respective controls. *P* values less than 0.05 were considered significant.

Results

Loading capacity of GO/DOX and rGO/FA/DOX conjugates

The loading percentage of DOX onto GO as the passive form (GO/DOX) was 91%. In the active form (rGO/FA/DOX), the loading percentage of DOX and FA was 83% and 54% (Fig. 2a).

FT-IR spectra of the conjugates

Typical FT-IR spectrum of GO is presented in (Fig. 2b). The characteristic peaks of GO are observed as broad peak at 3430 cm^{-1}confirming the stretching of O-H group, However, the peak at 2904 cm^{-1} indicated a O-H of carboxylic acid group and the peak at 1733 cm^{-1}showed the stretch C=O of ketone and aldehyde groups. Characteristic peaks at 1633 cm^{-1} depicted the presence of amino groups (-NH bands) and aldehyde C=O stretches onto GO surface explaining the loading of DOX. The alcoholic group was shifted to 3446 cm^{-1}, strong stretch C=O band of ketone and the aldehyde groups was shifted to 1741 cm^{-1}, and bend N-H band of amine and amide groups shifted to 1617 cm^{-1}, The presence of 1393 cm^{-1} band indicated to alkyl halide group of stretch C-O band of alcoholic group shifted to 1069 cm^{-1} due to DOX capping onto GO sheets via weak electrostatic interactions. The band at 605 cm^{-1} showed aromatic C-H band arising out of hydrophobic benzene rings in the DOX molecule.

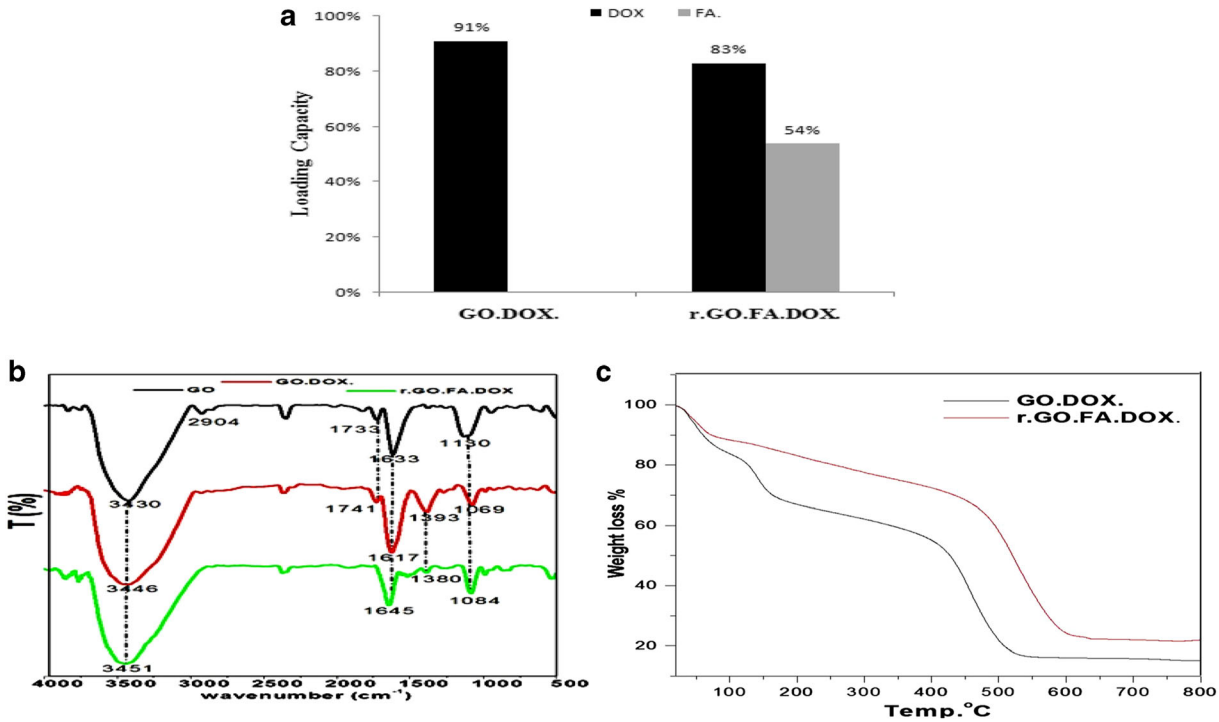

Fig. 2 **a** Loading capacity percentage of DOX onto GO to form GO/DOX and onto rGO/FA to form rGO/FA/DOX conjugates. **b** FT-IR characteristic FT-IR peaks of DOX loaded on GO and rGO/FA/DOX. **c** TGA analysis of GO/DOX and rGO/FA/DOX conjugate

Finally, the characteristic peaks of rGO/FA/DOX observed as stretch hydrogen–bond, O-H band of alcoholic group shifted to 3451 cm^{-1}, stretch C=O band of ketone and aldehyde groups shifted to 1645 cm^{-1}.

Thermogravimetric analysis of the conjugates

Thermogravimetric analysis (TGA) curves of the pure GO/DOX and rGO/FA/DOX are shown in (Fig. 2c). The curve GO/DOX showed a weight loss in 5 steps with total weight loss (83 wt %). The first weight loss (14 wt %) is at low temperature (< 100 °C) and it can be assigned to the loss of the residual adsorbed solvent. The major weight loss at the onset of 511 °C with (34 wt %) and this could be attributed to the breakdown of the carbon-oxygen contents. When the temperature reached 800 °C, the remained 17 wt % and almost no weight loss occurred after this temperature. For the rGO/FA/DOX, the weight loss displayed on four steps with total weight loss 78 wt %. The slow weight loss, 9.88 wt %, at low temperature < 100 °C can be attributed to evolved adsorbed solvent. The large weight loss was observed at the onset of 588 °C with weight loss (42 wt %) that may be referred to the breakdown of the –COO. A weight loss of approximately 50% was observed between 280 and 320 °C, possibly due to the loss detachment of FA. These results revealed that the thermal properties of DOX-loaded GO were dominated by the DOX content.

TEM measurements of the conjugates

The morphological analyses of pristine GO, GO/DOX, and rGO/FA/DOX were examined by TEM measurements. Figure 3 displays the images of GO, GO/DOX, and r-GO/FA/DOX, where it clearly shows the two-dimensional structure with some wrinkles on the surface and a sheet nature which ensures that morphology of GO was stable (Fig. 3).

In vitro antitumor effects of free DOX versus conjugates

As shown in (Fig. 4a), when GO/DOX or rGO/FA/DOX conjugates was added to EAC cell culture, they were precipitated as dark aggregations as indicated by inverted microscope. We then used MTT assay to assess the viability of EAC tumor cells after their treatment in vitro with 50 μg/ml of DOX or GO/DOX or rGO/FA/DOX conjugates for 48 h. The viability of EAC cells was decreased by 24%, 68%, and 75% after treatment

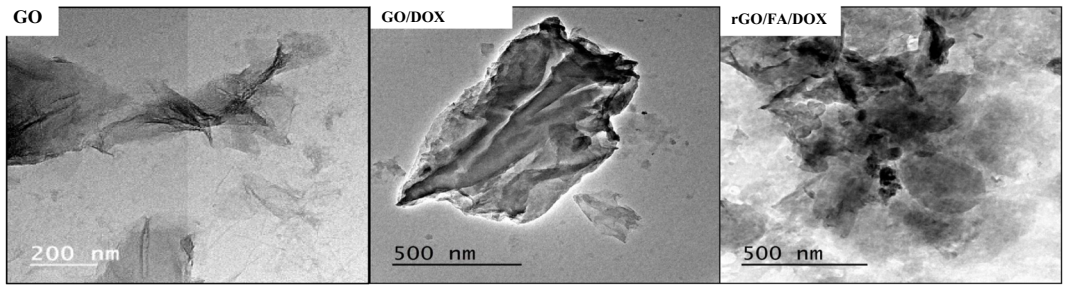

Fig. 3 TEM images of conjugates showing GO (left), GO/DOX (middle), and rGO/FA/DOX (right)

with free DOX, rGO/FA/DOX, and GO/DOX, respectively, relative to the PBS-treated EAC cells (Fig. 4b).

In vivo antitumor activities of free DOX versus conjugates

EAC-bearing mice were i.p. injected with DOX or conjugates. The results revealed that treatment of EAC-bearing mice with DOX, GO/DOX, or rGO/FA/DOX significantly induced reduction in the total number of tumor cells by 46-fold, 5-fold, and 28-fold, respectively comparing with PBS-tread mice (Fig. 5), indicating that rGO/FA/DOX conjugate is more effective than GO/DOX.

Effects of free DOX versus conjugates on EAC cell cycles

When EAC-bearing mice were treated with free DOX, EAC cell cycle was arrested at G0 phase (80.8%). In case of treatment with GO/DOX and rGO/FA/DOX forms, EAC cell cycle was arrested at G1 phase (50.9%) and S phase (46.2%), respectively (Fig. 6).

Effects of free DOX versus conjugates on apoptosis of EAC cells

Evaluation of apoptosis of EAC tumor cells collected from EAC-bearing mice treated with free DOX, GO/DOX, and rGO/FA/DOX was assessed by annexin/PI staining by flow cytometry. The results showed that active form rGO/FA/DOX induced significant increase of early apoptotic percentage (7%) compared with free DOX (4%). rGO/FA/DOX induced significant increase of late apoptotic percentage (70%) compared with free DOX (44%). When treatment with GO/DOX passive form induced a significant increase in necrotic cell percentage (26%) as compared with free DOX (4%) and rGO/FA/DOX active form (7%) (Fig. 7).

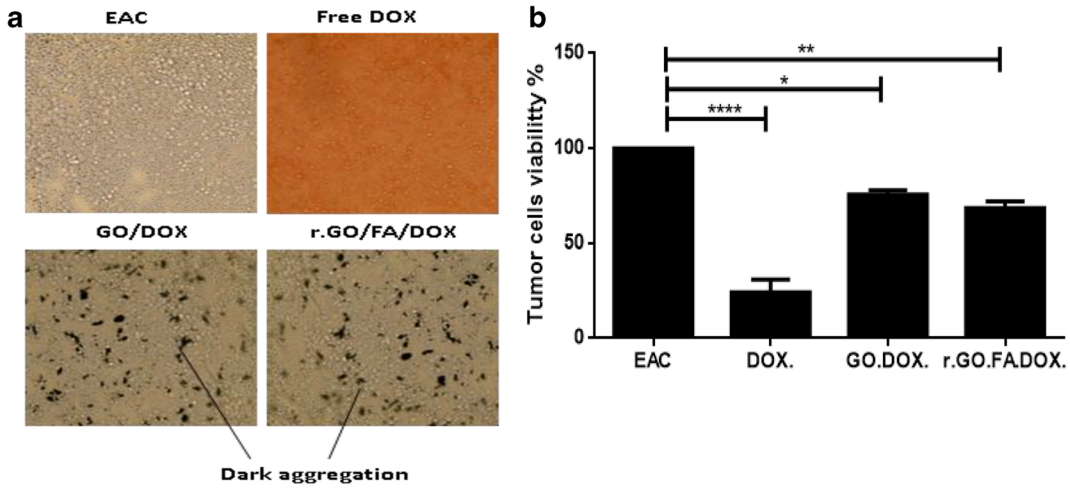

Fig. 4 Effect of GO/DOX and rGO/DOX/FA conjugates on tumor cell viability. EAC cells were cultured in vitro for 48 h and then assessed under inverted microscope and then stained with trypan blue for viability assay. **a** The culture with the conjugates displayed dark aggregations (lower panel). Data are represented as mean ± SE ($n = 3$). * $P \leq 0.05$, ** $P \leq 0.01$, **** $P \leq 0.0001$ statistically significant comparison of control group and other treated groups

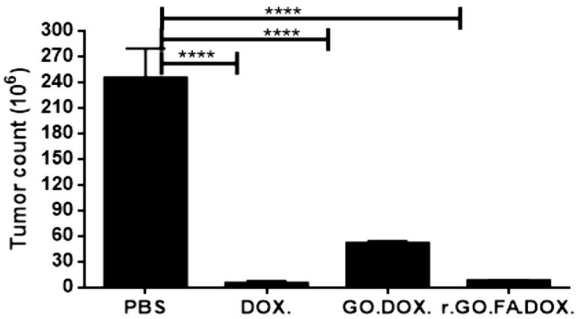

Fig. 5 Antitumor effects of GO/DOX and rGO/DOX/FA conjugates on tumor cell viability. CD1 mice ($n = 8$) were challenged intraperitoneally with 2.5×10^5 viable EAC cells. After 24 h of tumor challenge, EAC-bearing mice were treated with GO/DOX, rGO/FA/DOX, free DOX, or PBS. The dose of DOX in conjugated was adjusted. Mice were sacrificed on day 10 and EAC cells were harvested from the peritoneal ascites. The total numbers of EAC cells were counted by hemocytometer using trypan blue assay. Data are represented as mean ± SE ($n = 3$), **** $P \leq 0.0001$ statistically significant comparison of control group and other treated groups

Discussion

Our results showed that the active form of GO conjugate (rGO/FA/DOX) induced higher antitumor effect than the passive form. Interestingly, the passive and active form (GO/DOX) showed different trans on tumor cell cycle and apoptosis.

Given the applicability of GO as a potential drug delivery system, we compared in this study the antitumor efficacy of free DOX and conjugated DOX with GO alone (passive) or in combination with FA (active). Our results showed that conjugation of DOX with GO alone or in the presence of FA did not interfere with the antitumor effect of DOX both in vitro and in vivo. Taken together, our results indicate to the potential of conjugation of GO with anticancer chemotherapeutic drugs in particular aromatic structure drugs.

In our study, we found that the loading capacity of DOX on GO reached 91% which is consistent with the previous study which recorded over 90% conjugation of GO with DOX (Chen et al. 2014). This conjugation on one hand could be explained mainly through π-π stacking interaction (Zhao et al. 2011). On the other hand, it could be explained as the $-NH_2$ groups of DOX is expected to form additional hydrogen bonding with GO which was confirmed by FT-IR spectrum. However, in the presence of FA, the loading of DOX reached only 83%. This reduction in the loading capacity could be explained by chemical manipulation of GO during its reduction to form rGO when the majority of the oxygenated functional groups are removed to make a space

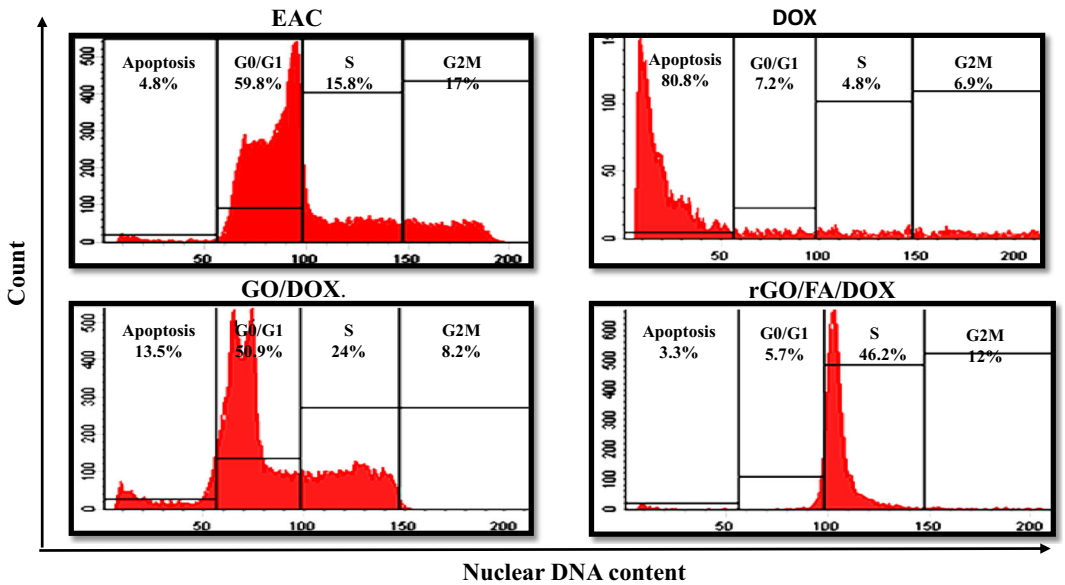

Fig. 6 Effects of GO/DOX and rGO/DOX/FA conjugates on tumor cell cycle. CD1 mice ($n = 8$) were challenged intraperitoneally with 2.5×10^5 viable EAC cells. After 24 h of tumor challenge, EAC-bearing mice were treated with GO/DOX, r/GO/FA/DOX, free DOX, or PBS. The dose of DOX in conjugated was adjusted at 15 mg/kg. Mice were sacrificed on day 10 and EAC cells were harvested from the peritoneal ascites. Equal numbers of EAC cells were used for cell cycle assay using flow cytometry after their staining with propidium iodide (PI). Cells were analyzed by flow cytometry for the marker indicated on the representative histograms

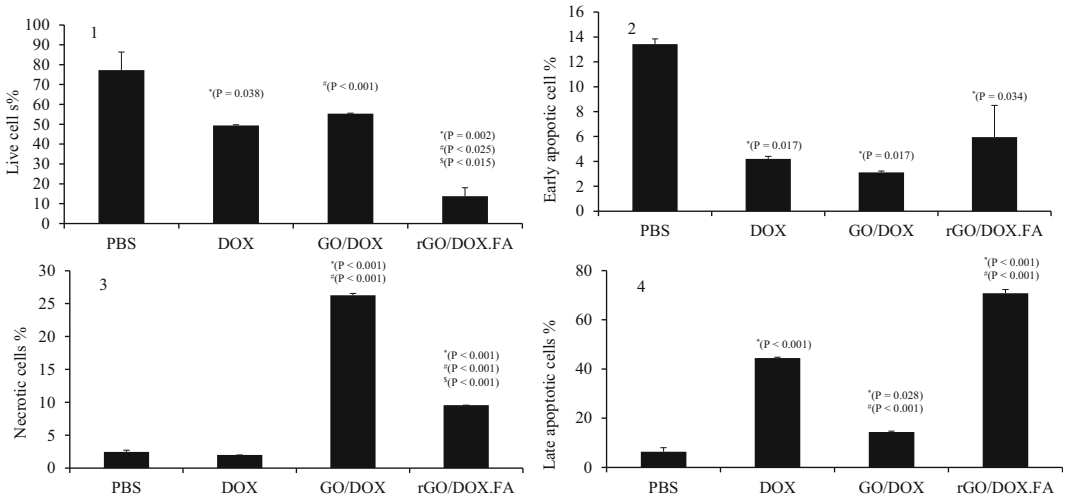

Fig. 7 Effects of GO/DOX and rGO/DOX/FA conjugates on tumor cell apoptosis. CD1 mice ($n = 8$) were challenged intraperitoneally with 2.5×10^5 viable EAC cells. After 24 h of tumor challenge, EAC-bearing mice were treated with GO/DOX, r/GO/FA/DOX, free DOX, or PBS. The dose of DOX in conjugated was adjusted. Mice were sacrificed on day 10 and EAC cells were harvested from the peritoneal ascites. Equal numbers of EAC cells were used for apoptosis assay using flow cytometry after their staining with annexin-V and PI. Statistical analysis of viable cells (upper left), early apoptotic cells (upper right), necrotic cells (lower left), and late apoptotic cells (lower right)

for FA (Akhavan et al. 2012) or the competition between FA and on GO surface.

To compare the antitumor efficacy of free DOX and conjugated DOX, we used in vitro and in vivo systems. We used the in vitro system to address whether the conjugates possess direct antitumor effect as free DOX. As expected, DOX showed strong antitumor effect as measured by MTT cell viability. In line with previous studies which reported that GO/DOX conjugates had antitumor effects on different cancer cell lines (Fong et al. 2017), our in vitro results also showed that DOX conjugation with GO resulted in appreciated antitumor effects on EAC cells. However, both the passive (GO/DOX) and active (rGO/FA/DOX) conjugates showed lower cytotoxic effect on EAC as compared with free DOX. Although it is not clear why conjugates of DOX resulted in this lower antitumor effect, it could be suggested due to different mechanisms. One possible mechanism could be that the release of DOX from GO takes longer time than free DOX. Additionally, conjugates behave as a colloid and may react with the culture media and form protein corona (McCallion et al. 2016) which may disturb the culture microenvironment such as nutrients and PH (Mahmoudi et al. 2010). This is likely to be a working hypothesis, as we found dark aggregations between the cultured cells. (Fig. 4a).

Opposite to the in vitro results, our in vivo studies showed that the antitumor effects of the conjugates are similar to those of free DOX as indicated by the decrease in the total number of tumor cells after treatment. Of note, we found in our study that the active form of the conjugate (rGO/FA/DOX) showed higher antitumor effect than its passive form (GO/DOX). The higher effect of active versus passive form could be explained by the possibility of binding of FA to its membrane-bound receptor (FA receptor) which acts as cellular transporter for FA (Kamen and Capdevila 1986), where FA is uptaken into the cytosol through endocytosis (Low et al. 2008). Our results are in line with the previous studies which showed overall that the antitumor effect of the active GO is superior to its passive form against several tumors. For instance, the encapsulated hyaluronic acid-chitosan-g-poly N-isopropylacrylamide (HACPN) GO/FA/DOX/HACPN showed higher antitumor efficacy against xenograft breast tumor (MCF-7; MCF-7/Luc cells) than its passive form (Fong et al. 2017). Since, it was also found that rGO/FA/DOX nanosheets coated with an antiangiogenic anticancer derivative of low-molecular-weight heparin (LHT7) showed the greatest antitumor effect in tumor bearing, suggesting that the nano carriers conjugated with FA can be targeted to tumor cells and internalized through receptor-mediated endocytosis (Prabaharan et al. 2009; Stella et al. 2000).

Anticancer compounds demonstrate their antitumor effect either by arresting the cell growth at a specific

checkpoint of cell cycle or by induction of apoptosis Gerard and Karen (2001). The efficacy of GO/FA/DOX and GO/DOX to induce apoptosis of MCF7 cells and multiple myeloma in vitro was reported (Fong et al. 2017; Wu et al. 2014). As such, we analyzed the impact of treatments with conjugates on these two parameters. Regarding cell cycle, we found that GO/DOX and rGO/FA/DOX treatments arrested the cell cycle at G1 and S phase, respectively. Treatment with free DOX, however, induced tumor cell cycle arrest at sub-G0 phase. Previous studies showed that GO and rGO induce cell cycle arrest at the G0/G1 phase suggesting that active GO causes more potent toxic effects than reduced GO (Khan et al. 2016; Matesanz et al. 2013). Consistent with this notion, previous studies also showed that treatment with nanomaterials may lead to cell cycle arrest at various phases (Liu et al. 2017; Patel et al. 2016). With regard to apoptosis, the current study showed that as compared with the anti-apoptotic effects of free DOX, rGO/FA/DOX treatment induced significant increases in the early and late apoptotic EAC cells in contrast with GO/DOX which caused high induction of necrotic cells. Late apoptotsis is considered to be a good marker to the antitumor effect of compound than necrosis. These data suggest that the antitumor effects of conjugates are mediated by both arresting tumor cell cycle and induction of apoptosis.

In conclusion, the data of the current study indicate that although conjugates had similar antitumor effects as free DOX, their effects on cell cycle and apoptosis are different. These results open new door for investing the cellular and molecular mechanisms of these conjugates as well as to compare its adverse effects with those of DOX.

Compliance with ethical standards

Conflict of interest The authors declare that they have no conflict of interest.

References

Akhavan O, Ghaderi E, Akhavan A (2012) Size-dependent genotoxicity of graphene nanoplatelets in human stem cells. Biomaterials 33:8017–8025. https://doi.org/10.1016/j.biomaterials.2012.07.040

Bhatia S (2016) Nanoparticles types, classification, characterization, fabrication methods and drug delivery applications in natural polymer drug delivery systems: nanoparticles, plants, and algae. Springer International Publishing, Switzerland, pp 33–93. https://doi.org/10.1007/978-3-319-41129-3_2

Chen Y et al (2014) Multifunctional graphene oxide-based triple stimuli-responsive. Nanotheranostics Adv Funct Mater 24: 4386–4396

Coffelt SB, de Visser KE (2015) Immune-mediated mechanisms influencing the efficacy of anticancer therapies. Trends Immunol 36:198–216. https://doi.org/10.1016/j.it.2015.02.006

Daniels TR, Delgado T, Rodriguez JA, Helguera G, Penichet ML (2006) The transferrin receptor part II: targeted delivery of therapeutic agents into cancer cells. Clin Immunol 121:159–176

Dinauer N, Balthasar S, Weber C, Kreuter J, Langer K, von Briesen H (2005) Selective targeting of antibody-conjugated nanoparticles to leukemic cells and primary T-lymphocytes. Biomaterials 26:5898–5906. https://doi.org/10.1016/j.biomaterials.2005.02.038

Fong YT, Chen CH, Chen JP (2017) Intratumoral delivery of doxorubicin on folate-conjugated graphene oxide by in-situ forming thermo-sensitive hydrogel for breast cancer therapy. Nanomaterials (Basel) 7:388. https://doi.org/10.3390/nano7110388

Geim AK, Novoselov KS (2007) The rise of graphene. Nat Mater 6:183–191

Gerard EI, Karen VH (2001) Proliferation, cell cycle and apoptosis in cancer. Nature 411:342–348

Janes KA, Calvo P, Alonso MJ (2001) Polysaccharide colloidal particles as delivery systems for macromolecules. Adv Drug Deliv Rev 47:83–97

Kamen BA, Capdevila A (1986) Receptor-mediated folate accumulation is regulated by the cellular folate content. Proc Natl Acad Sci U S A 83:5983–5987. https://doi.org/10.1073/pnas.83.16.5983

Khan M et al (2016) Apoptosis inducing ability of silver decorated highly reduced graphene oxide nanocomposites in A549 lung cancer. Int J Nanomedicine 11:873–883. https://doi.org/10.2147/IJN.S100903

Khan MS, Pandey S, Bhaisare ML, Gedda G, Talib A, Wu HF (2017) Graphene oxide@gold nanorods for chemo-photothermal treatment and controlled release of doxorubicin in mice. Tumor Colloids Surf B Biointerf 160:543–552. https://doi.org/10.1016/j.colsurfb.2017.09.001

Kim KJ, Joe YA, Kim MK, Lee SJ, Ryu YH, Cho DW, Rhie JW (2015) Silica nanoparticles increase human adipose tissue-derived stem cell proliferation through ERK1/2 activation. Int J Nanomedicine 10:2261–2272. https://doi.org/10.2147/IJN.S71925

Licciardi M, Giammona G, Du J, Armes SP, Tang Y, Lewis AL (2006) New folate-functionalised biocompatible block copolymer micelles as potential anti-cancer drug delivery systems. Polymer 47:2946–2955. https://doi.org/10.1016/j.polymer.2006.03.014

Liu J, Kang Y, Zheng W, Song B, Wei L, Chen L, Shao L (2017) Ion-shedding zinc oxide nanoparticles induce microglial BV2 cell proliferation via the ERK and Akt signaling pathways. Toxicol Sci 156:167–178

Low PS, Henne WA, Doorneweerd DD (2008) Discovery and development of folic-acid-based receptor targeting for imaging and therapy of cancer and inflammatory diseases. Acc Chem Res 41: 120–129. https://doi.org/10.1021/ar7000815

Mahmoudi M, Simchi A, Imani M, Shokrgozar MA, Milani AS, Hafeli UO, Stroeve P (2010) A new approach for the in vitro identification of the cytotoxicity of superparamagnetic iron

oxide nanoparticles. Colloids Surf B: Biointerfaces 75:300–309. https://doi.org/10.1016/j.colsurfb.2009.08.044

Marcano DC et al (2010) Improved synthesis of graphene oxide. ACS Nano 4:4806–4814. https://doi.org/10.1021/nn1006368

Matesanz MC et al (2013) The effects of graphene oxide nanosheets localized on F-actin filaments on cell-cycle alterations. Biomaterial 34:1562–1569

McCallion C, Burthem J, Rees-Unwin K, Golovanov A, Pluen A (2016) Graphene in therapeutics delivery: problems, solutions and future opportunities. Eur J Pharm Biopharm 104: 235–250. https://doi.org/10.1016/j.ejpb.2016.04.015

Minotti G, Menna P, Salvatorelli E, Cairo G, Gianni L (2004) Anthracyclines: molecular advances and pharmacologic developments in antitumor activity and cardiotoxicity. Pharmacol Rev 56:185–229. https://doi.org/10.1124/pr.56.2.6

Muazim K, Hussain Z (2017) Graphene oxide-a platform towards theranostics. Mater Sci Eng C Mater Biol Appl 76:1274–1288. https://doi.org/10.1016/j.msec.2017.02.121

Nasongkla N, Shuai X, Ai H, Weinberg BD, Pink J, Boothman DA, Gao J (2004) cRGD-functionalized polymer micelles for targeted doxorubicin delivery. Angew Chem Int Ed Eng 43: 6323–6327. https://doi.org/10.1002/anie.200460800

Osman AM, al-Harthi SE, AlArabi O, Elshal MF, Ramadan WS, Alaama MN, al-Kreathy HM, Damanhouri ZA, Osman OH (2013) Chemosensetizing and cardioprotective effects of resveratrol in doxorubicin-treated animals. Cancer Cell Int 13: 52. https://doi.org/10.1186/1475-2867-13-52

Patel P, Kansara K, Senapati VA, Shanker R, Dhawan A, Kumar A (2016) Cell cycle dependent cellular uptake of zinc oxide nanoparticles in human epidermal cells. Mutagenesis 31: 481–490. https://doi.org/10.1093/mutage/gew014

Prabaharan M, Grailer JJ, Pilla S, Steeber DA, Gong S (2009) Amphiphilic multi-arm-block copolymer conjugated with doxorubicin via pH-sensitive hydrazone bond for tumor-targeted drug delivery. Biomaterials 30:5757–5766. https://doi.org/10.1016/j.biomaterials.2009.07.020

Siriviriyanun A, Popova M, Imae T, Kiew LV, Looi CY, Wong WF (2015) Preparation of graphene oxide/dendrimer hybrid carriers for delivery of doxorubicin. Chem Eng J 281:771–781. https://doi.org/10.1016/j.cej.2015.07.024

Stella B et al (2000) Design of folic acid-conjugated nanoparticles for drug targeting. J Pharm Sci 89:1452–1464. https://doi.org/10.1002/1520-6017(200011)89:11<1452::aid-jps8>3.0.co;2-p

Wu S, Zhao X, Cui Z, Zhao C, Wang Y, Du L, Li Y (2014) Cytotoxicity of graphene oxide and graphene oxide loaded with doxorubicin on human multiple myeloma cells. Int J Nanomedicine 9:1413–1421. https://doi.org/10.2147/IJN.S57946

Zhao GX, Li JX, Wang XK (2011) Kinetic and thermodynamic study of 1-naphthol adsorption from aqueous solution to sulfonated graphene nanosheets. Chem Eng J 173:185–190